ELSEVIER

International Journal of Heat and Fluid Flow 19 (1998) 594–600

International Journal of HEAT AND FLUID FLOW

The application of thin-film technology to measure turbine-vane heat transfer and effectiveness in a film-cooled, engine-simulated environment

S.M. Guo [a,*], C.C. Lai [a], T.V. Jones [a], M.L.G. Oldfield [a], G.D. Lock [b], A.J. Rawlinson [c]

[a] *Department of Engineering Science, University of Oxford, Parks Road, Oxford, OX13PJ, UK*
[b] *Department of Mechanical Engineering, University of Bath, Bath, BA2 7AY, UK*
[c] *Rolls Royce plc, Turbine Engine Systems, PO Box 31, Derby, DE24 8BJ, UK*

Received 27 September 1997; accepted 9 May 1998

Abstract

Thin-film technology has been used to measure the heat transfer coefficient and cooling effectiveness over heavily film cooled nozzle guide vanes (NGVs). The measurements were performed in a transonic annular cascade which has a wide operating range and simulates the flow in the gas turbine jet engine. Engine-representative Mach and Reynolds numbers were employed and the upstream free-stream turbulence intensity was 13%. The aerodynamic and thermodynamic characteristics of the coolant flow (momentum flux and density ratio between the coolant and mainstream) have been modelled to represent engine conditions by using a foreign gas mixture of SF_6 and Argon. Engine-level values of heat transfer coefficient and cooling effectiveness have been obtained by correcting for the different molecular (thermal) properties of the gases used in the engine-simulated experiments to those which exist in the true engine environment. This paper presents the best combined heat transfer coefficient and effectiveness data currently available for a fully cooled, three-dimensional NGVs at engine conditions.

Keywords: Heat transfer; Film cooling; Nozzle guide vane; Thin film gauge; Engine simulation; Gas turbine

Notation

Cp	specific heat at constant pressure
h	heat transfer coefficient
k	thermal conductivity
M	molecular weight
Ma	Mach number
P	pressure
q	heat transfer rate
R	gas constant
Re	Reynolds number
t	time
T	temperature
x	axial chord

Greek

ρ	density
η	film cooling effectiveness
β	thermal diffusivity
γ	ratio of specific heats
ζ	concentration

Subscripts

aw	adiabatic wall
c	coolant
e	engine
m	gas, mainstream
mole	molar
o	total, stagnation
r	recovery
s	surface
w	wall
x	experiment

1. Introduction

The efficiency and specific thrust of gas turbine engines increase with higher gas temperature after combustion and typical modern aeroengines experience turbine entry temperatures of up to 1700 K. In practice there are no metals for turbine components that will withstand uncooled operation at these elevated gas temperatures. At such temperatures the turbine blade must be safeguarded against the hot gases and film cooling is one of the major methods employed. Cooling technology involves the use of relatively cool air which is taken from the compressor exit and bypasses the combustion process to cool the vanes through rows of discrete cooling holes. Meece (1995) reported that a cooling effectiveness of 0.6

* Corresponding author. E-mail: shengmin.guo@eng.ox.ac.uk.

0142-727X/98/$00.00
PII: S0142-727X(98)10034-6

can be achieved by using advanced film cooling technology, which allows an inlet temperature of 1900 K for single crystal blades.

There is a vast quantity of experimental and computational work on the topic of gas turbine film cooling, dating back to the 1940s (Goldstein, 1971; Hartnett, 1985). Several different measurement techniques have been employed to obtain film cooling data. The heat-mass transfer analogy is used in the Swollen Polymer (Hay et al., 1984) and Naphthalene Sublimation (Cho and Goldstein, 1995; Richter et al., 1996) techniques to determine heat transfer coefficient and effectiveness. Effectiveness alone may also be found using gas concentration techniques of which the Ammonia and Diazo (Friedrichs et al., 1995; Haslinger and Hennecke, 1996) technique is an example. Thin film gauges (Jones, 1995), thermochromic liquid crystals (e.g., Drost et al., 1997), infra-red thermography (Giebert et al., 1997) or thermocouples on adiabatic surfaces (Goldstein et al., 1968) provide surface temperature measurements in either a transient or steady-state manner. The latter techniques enable heat transfer coefficient and effectiveness to be obtained.

The quantities of interest in film cooling experiments are the convective heat transfer coefficient (h) and the film effectiveness (η). The former is the constant of proportionality between the local heat flux (q) and the difference between the surface temperature (T_s) and convection driving temperature of the gas (T_{aw}, or *adiabatic wall temperature*) at that point:

$$q = h(T_s - T_{aw}). \tag{1}$$

The adiabatic wall temperature is chosen since it is desirable to define, and measure, a heat transfer coefficient which is independent of the temperature boundary conditions and a function of the aerodynamic character of the flowfield alone. This is not strictly possible as there are well known and predictable differences between an isothermal wall situation and a constant heat flux boundary condition. However, for small streamwise gradients in temperature and constant fluid properties it has been found that a wall temperature variation has only a minor influence on local convective heat transfer (Eckert et al., 1957; Butler and Baugh, 1996). For two-temperature convection cases (i.e. without a separate coolant flow) T_{aw} is the local gas recovery temperature. In film cooling, with two flows present, T_{aw} is intermediate between the coolant (T_{oc}) and mainstream (T_{om}) total temperatures, and depends upon the geometry and degree of mixing between these gases upstream of the point of interest on the surface. To eliminate the temperature dependence a conventional dimensionless adiabatic film effectiveness is defined for constant property compressible flow on an adiabatic surface

$$\eta = \frac{T_{aw} - T_r}{T_{oc} - T_r}, \tag{2}$$

where T_r is the local mainstream gas recovery temperature. An alternative definition of cooling effectiveness, based on superposition (Jones, 1991) and similar to the isoenergetic definition of Eckert (Goldstein, 1971), is used here,

$$\eta = \frac{T_{aw} - T_r}{T_{oc} - T_{om}}, \tag{3}$$

where T_{aw} corresponds to the temperature of an isothermal wall which is adiabatic at the local point of interest. In practice there is only a small difference in the results using either definition.

The cooling effectiveness and heat transfer coefficient are a function of the following: cooling geometry (the angles of inclination and orientation, the relative spacing of the coolant holes, the hole shape); the state of the oncoming boundary layer; the freestream turbulence intensity; the surface curvature; and the ratios of the coolant-to-mainstream density, mass and momentum fluxes, and specific heats. There are very few film cooling studies where measurements are made in an engine-representative environment.

This paper will demonstrate the application of thin film gauges to the film-cooled gas turbine situation. The gauges have been designed and manufactured at Oxford. They feature technology which differs from that associated with conventional heat transfer gauges as the thin-film sensors are located on thin, flexible polyimide sheets which can be adhesively bonded to perspex models of film-cooled nozzle guide vanes. These vanes form the test section of short-duration tunnel which creates steady engine-representative conditions in a transonic annular cascade. Heavy coolant gases are used to simulate the coolant-to-mainstream density ratio which exists in the engine. The thin-film gauges provide surface-temperature histories around the mid-span of the vanes from a transient (3–5 s) experiment. Standard analysis techniques are employed to yield the heat-flux history, and thus the steady-state heat transfer coefficient and film cooling effectiveness. These measurements are then scaled to those which would exist in the true engine environment by correcting for the different molecular (thermal) properties of the gases used in the engine-simulated experiment.

2. Nozzle guide valves cooling geometry

The NGV under investigation is from the first stage turbine (downstream of the combustor) of a modern Rolls-Royce aeroengine. The cooling configuration consists of fourteen rows with a total of approximately 350 cooling holes. The holes are fed from one of two internal cavities, as illustrated in Fig. 1. These cavities are independently supplied with coolant so as to maintain the engine coolant-to-mainstream total pressure ratios, $P_{oc}/P_{om} = 1.02$. This pressure ratio is fixed and determined by the loss in pressure between the compressor exit and vane compared with that lost for the flow which passes through the combustor. The forward cavity supplies 12 of the 14 rows, a total of almost 300 cooling holes, positioned around the leading edge, the early regions of the pressure surface and suction surface. The rear cavity feeds two rows, a total of approximately 50 cooling holes, nearest the trailing edge on the pressure surface.

The range of flow conditions encountered at the film-cooling hole exits around the vane surface is significant; the mainstream Mach number varies between 0.04 and 0.96, the pressure ratio across the holes, P_{oc}/P_{om}, varies between 1.02

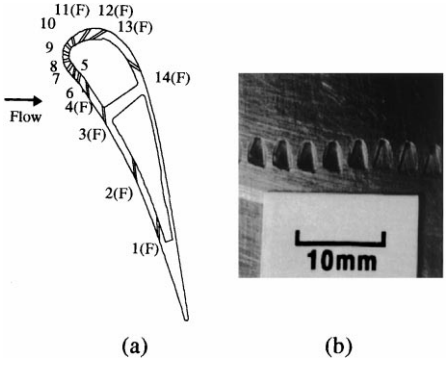

Fig. 1. (a) Mid-span cross-section of a CHTT NGV having the full film cooling geometry, illustrating row positions and two-cavity construction. The holes marked (F) are fan-shaped in the fan-shaped geometry; (b) Close view of the fan-shaped holes.

and 1.77, and length-to-diameter ratios of the holes varies between 3.5 and 10.3. The two commonly defined hole angles (see for example, Hay and Lampard, 1995), the angles of inclination and orientation vary within the ranges 20–90° and 0–60°, respectively.

The NGV was manufactured on a five-axis NC milling machine from engineering drawings supplied by Rolls-Royce. Two film cooling geometries were tested. The first was with all holes cylindrically shaped. The second was with rows 1–4 and 11–14 fanshaped. Hay and Lampard (1995) have discussed the benefits of fan-shaped coolant holes, which include: enhanced lateral spreading of the jets over the blade surface compared with cylindrical holes; the slowing down of the jets through diffusion in the fans, permitting higher injection rates before jets lift-off occurs; and a greater discharge coefficient of the fan-shaped holes, compared with the equivalent cylindrical holes, which give a lower pressure drop for a given mass flow.

3. Experimental Apparatus

3.1. Film cooling test facility

The measurements were conducted in the Oxford University Cold Heat Transfer Tunnel (CHTT). The test section of the tunnel is an annular cascade of 36 NGVs at 1.4 times larger than engine scale. The tunnel and application of the transient liquid crystal technique to measure heat transfer on the aerofoil surfaces (Martinez-Botas et al., 1995) and endwalls (Spencer et al., 1996) are described elsewhere. The NGV instrumented with the thin film gauges and its immediate neighbours can be either preheated or precooled before the test begins. The tunnel is part of a blowdown facility with the main reservoir at room temperature. The test duration is typically 3–5 s. The tunnel allows an independent variation of Reynolds and Mach numbers, or equivalently the upstream and downstream pressures of the cascade can be independently and continuously varied. All of the results presented here are at engine design condition ($Re_{exit} = 2 \times 10^6$, based on axial chord and exit conditions, and $Ma_{exit} = 0.96$) and with a free-stream turbulence intensity and length scale of 13% and 21 mm at NGV inlet.

The experiments were designed to model the engine situation where the coolant is at a lower temperature, and hence more dense, than the mainstream flow. It has been demonstrated (Teekaram et al., 1989) that this density ratio can be simulated using a heavy, foreign gas. A mixture of SF_6 (30.2% by weight) and Ar (69.8% by weight) is used here which has the same ratio of specific heats ($\gamma = 1.4$) but is 1.77 times more dense than air. By matching the total pressure ratio of coolant to mainstream, the velocity ratio and density ratio can be made to correspond to engine conditions. Thus mass flux ratio and momentum flux ratio are also identical.

Coolant is supplied to the 36 NGVs through calibrated metering orifices. Thirty-three of the vanes have a simplified coolant geometry, while three test vanes have the full coolant geometry discussed above. Both air and foreign gas are available as coolant from high pressure reservoirs. The gas in these reservoirs can be preheated to satisfy thermal boundary conditions in the heat transfer experiments. Because the external heat transfer is the subject of the study, the coolant temperature was set equal to the initial temperature of the NGV to minimise internal heat transfer within the film cooling holes. The coolant total temperature varied by less than 2°C over the course of the experiment. The influence of such variation in the measurement of external heat transfer can be taken into account (Drost et al., 1997) but with such small variation the influence was ignored.

Table 1
Engine/tunnel comparison

Parameter	Engine	CHTT
Inlet total pressure (bar)	32	2
Coolant pressure ratio (P_{oc}/P_{om})	1.02	1.02
Turbine inlet temperature (K)	1750–1800	290
[a] Exit Reynolds number	2×10^6	2×10^6
Exit Mach number	0.96	0.96
Mainstream mass flow rate (kg/s)	120	38

[a] Based on axial chord and exit flow conditions.

Freestream Mach number and Reynolds number were simulated as previously mentioned and the coolant to mainstream density was also the same as the engine. Reynolds number and Mach number were based on freestream conditions at exit. Table 1 compares operating conditions between the CHTT and engine.

3.2. Effectiveness and heat transfer at engine conditions

The experimental data collected here is to be used to validate CFD codes. Such codes can be used with identical thermal boundary conditions and gas properties (c, k, γ, R, etc.) to those used in the experiments. Beyond CFD code validation, the experiments employing the foreign gas can provide meaningful data to the engine designer because they were conducted in a manner to best model the fluid dynamics which exist in the engine: the flow fields are similar and so the distribution of coolant are the same. Engine-level values of heat transfer coefficient and effectiveness can be obtained by correcting for the different molecular (thermal) properties of the gases used to those which exist in the engine environment.

The engine heat transfer coefficient is thus approximately obtained by scaling that value measured in the CHTT (Jones, 1998)

$$h_e = h_x \frac{x_x}{x_e}\frac{k_e}{k_x}\frac{Cp_{wx}}{Cp_x}\frac{1 + 0.924\frac{Cp_{wx}}{Cp_x}\frac{k_x}{k_{wx}}}{1 + 0.924\frac{k_e}{k_{we}}}. \quad (4)$$

Here h_e and h_x the heat transfer coefficients, k_e and k_x the gas conductivities, Cp_e and Cp_x the gas specific heats in the engine and CHTT, and subscript w the wall value respectively. The gas at the wall is a mixture of both mainstream and coolant. The conductivity is determined to sufficient accuracy (Oldfield and Guo, 1997) by the relative mole fraction of concentration (ζ_{mole}) and evaluated at the wall temperature,

$$k = k_m(1 - \zeta_{mole}) + k_c\zeta_{mole}. \quad (5)$$

The adiabatic wall effectiveness is related to the concentration and specific heats at constant pressure of the mainstream and coolant gases (Cp_m and Cp_c) thus:

$$\zeta = \frac{\eta Cp_m}{(1-\eta)Cp_c + \eta Cp_m}, \quad (6)$$

where ζ is the concentration by mass.

The mole fraction of coolant concentration can be calculated from its weight fraction thus:

$$\zeta_{mole} = \frac{\zeta}{\zeta + (1-\zeta)\frac{M_c}{M_m}}, \quad (7)$$

where M_c and M_m are the molecular weights of coolant and mainstream.

Finally the engine-level effectiveness can be related to that measured in the CHTT,

$$\eta_e = \frac{\eta_x}{\eta_x + (1-\eta_x)\left(\frac{Cp_c}{Cp_m}\right)_x\left(\frac{Cp_m}{Cp_c}\right)_e}, \quad (8)$$

where the gas specific heats are evaluated at local recovery temperatures. Further discussion is to be published by Jones (1998).

The experiments were conducted with small gas to wall temperature differences and local fluid properties were taken at the wall temperature in calculating the heat transfer coefficient. The wall temperature variation in the transient experiment was not taken into account as this had little effect on the fluid properties due to the small temperature differences.

4. Thin film gauges

4.1. Thin film gauges

When placed on a substrate of known thermal properties, measurements of surface temperature history using thin film resistance thermometers, coupled with the appropriate analytical model, can lead to the calculation of the surface heat flux history. The use of such gauges for measuring heat transfer rates to turbine blades in short-duration transient cascade facilities is well documented (Schultz and Jones, 1973; Jones et al., 1993). As well as measuring the surface heat transfer rates, the interpretation of these high frequency signals can yield much useful information about the gas flow and boundary layers.

A variety of different types of surface thin film gauges have been reported. This paper describes the use of a new type of thin film heat transfer gauge which has been developed at the Osney Laboratory at Oxford by Jones and others (Jones, 1995). A schematic of the gauge is shown in Fig. 2. Platinum thin film sensors (<0.04 μm thick) and copper leads (<0.5 μm thick) have been deposited onto polyimide (upilex is the polyimide brand) sheets which are subsequently adhesively bonded to perspex or metal models using 3M doubled-sided glue. The sheets are 50 μm thick and extremely flexible. Consistent construction of these gauges means that the calibration difficulties involved with traditional two-layered gauges (Doorly and Oldfield, 1987) are avoided and only the temperature-resistance coefficient of the platinum sensor needs to be determined. The gauges can be manufactured in various sizes and patterns and in multiple arrays. The application of these gauges to measure heat transfer to perspex and aluminium NGVs at engine-representative conditions in the absence of film cooling has already been demonstrated (Guo et al., 1995).

For the film cooling application the flexible sheet of polyimide was wrapped around and glued to a perspex NGV. Due to the complex curvature of the model it was necessary to fit together several carefully shaped pieces of polyimide to create an aerodynamically smooth surface. Subsequently holes were drilled through the polyimide to produce the film cooling geometries (Fig. 3). Careful drilling was required and the holes were drilled in the underlying model before mounting the polyimide sheet. The use of numerically-controlled machines

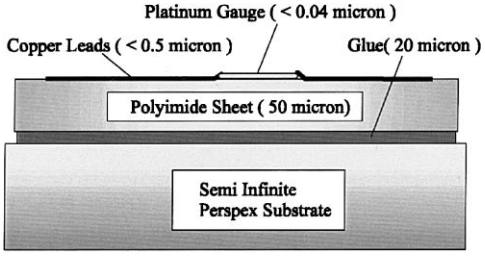

Fig. 2. Thin film gauge on polyimide (upilex) sheet.

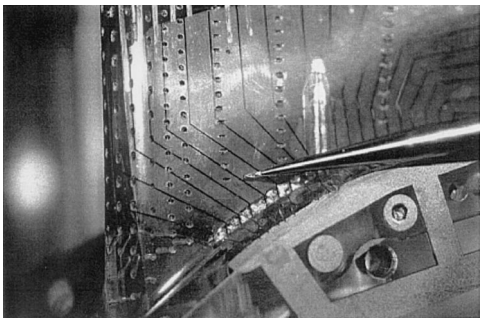

Fig. 3. Drilling of the film cooling holes through the polyimide sheet (the drill bit is shown approaching from the right).

to ensure accuracy in the process is essential. Great care was taken to make certain the film cooling holes were clear after the drilling was complete. A typical set of thin films had 18 gauges on both the pressure and suction surfaces, all aligned on a midspan streamline. The platinum gauge dimensions were 10 mm by 1.0 mm and were designed to cover the width of three film cooling holes. The measurements thus give a spanwise average of heat transfer downstream from the cooling holes. Fig. 4 shows the thin film gauges, copper leads and film cooling holes on the highly curved suction surface near the leading edge of the NGV.

A constant current source (Oldfield et al., 1984) was used to power the thin film gauges. The current was minimised to avoid significant heating of the thin films. The voltage histories of these gauges were amplified and then recorded at 2 kHz using an analogue to digital converter and computer. Higher frequency information can be obtained (on fewer channels) up to a rate of 300 kHz. Several thermocouples were used to measure the freestream and coolant total temperatures.

4.2. Data reduction

When operated in constant current mode, the voltage history from the gauges leads to measurements of the change in the gauge resistance with time. From the temperature–resistance calibration a measurement of the surface temperature history is obtained. When the polyimide sheet is mounted onto perspex models, the thin film gauges can be considered to be on a semi-infinite substrate because the thermal properties of the polyimide, glue and perspex are similar. When the polyimide sheet is mounted on a substrate with different thermal properties (e.g., metal), the system has to be analysed as a two-layered gauge (Doorly and Oldfield, 1987) (with the polyimide and

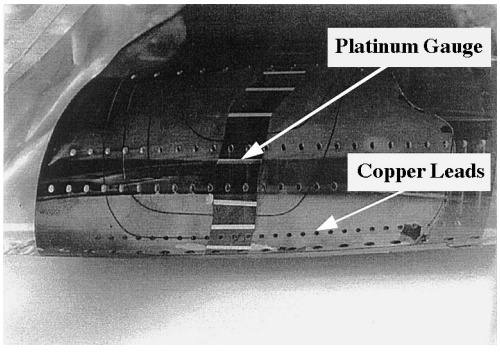

Fig. 4. Photograph of the thin film gauges and film cooling holes near the leading edge of the NGV.

glue a homogeneous material) or by using a finite-difference technique. Only the semi-infinite case will be discussed here.

The one-dimensional heat conduction equation

$$\frac{\partial^2 T_s}{\partial x^2} = \frac{1}{\beta}\frac{\partial T_s}{\partial t} \tag{9}$$

may be solved for the heat flux at the surface. Here t is time, x is the distance normal to the surface and β is the thermal diffusivity of the substrate. The assumption is made that the duration of the measurement is short enough that the penetration of the thermal pulse into the substrate is small when compared to the model dimensions. The boundary conditions are a uniform substrate temperature before the transient experiment begins and that the heat flux is proportional to the temperature gradient at the surface of the substrate, $q = -k\partial T_s/\partial_x$ where k is the thermal conductivity. The time variation of q may be evaluated using the method described in (Oldfield et al., 1978), viz.,

$$q(t) = q(m\tau) = 2\sqrt{\frac{\rho ck}{\pi\tau}} \times \sum_{n=0}^{m} (T_{n+1} + T_{n-1} - 2T_n)(m-n)^{0.5}, \tag{10}$$

where τ is the time interval between data points, m and n are integers, and $\sqrt{\rho ck}$ is the thermal product of substrate density, specific heat and conductivity.

4.3. Heat transfer coefficient and adiabatic wall temperature

A typical surface temperature history from a thin film gauge on the suction surface of a preheated NGV is shown in Fig. 5. The tunnel begins operation at 2.5 s and the surface temperature is seen to drop until the tunnel is shut off near 5 s. There is a fluctuation in surface temperature prior to 2.5 s as the coolant is activated beforehand. The heat transfer rate, calculated from Eq. (10), is shown as a function of surface temperature in Fig. 6. Note that the flow is steady (though highly turbulent), and hence the heat transfer coefficient is constant only between 28°C and 40°C. From Eq. (1), the gradient of this curve in that time segment yields the heat transfer coefficient. If the linear portion of this curve is extrapolated to $q = 0$ the intercept gives the local adiabatic wall temperature. The effectiveness is then obtained from Eq. (3).

5. Experimental results and discussion

Fig. 7 illustrates the measured isentropic Mach number distribution measured around the midspan on the pressure and suction aerofoil surfaces with the film cooling in operation.

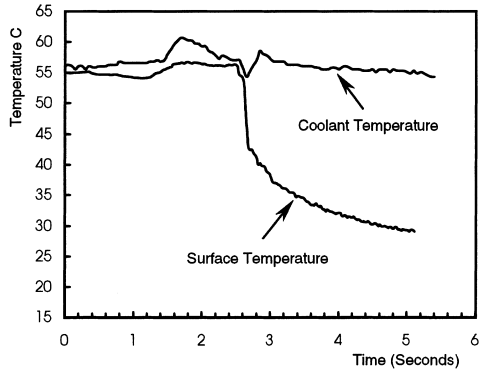

Fig. 5. Surface temperature history from thin film gauge.

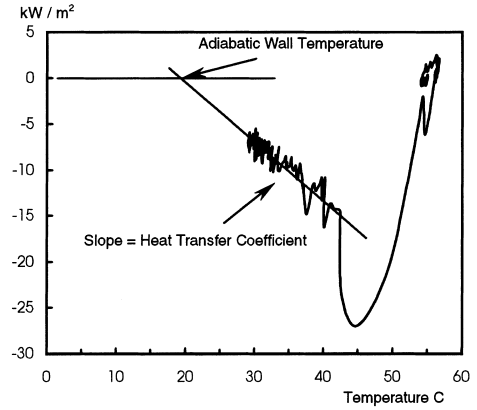

Fig. 6. Heat flux as a function of surface temperature.

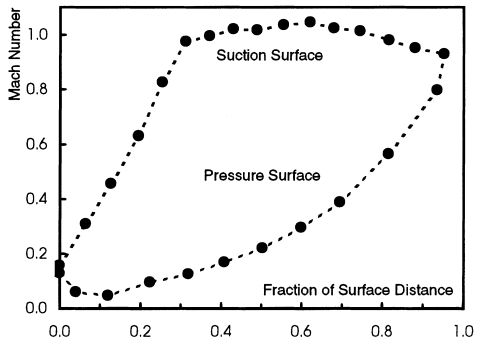

Fig. 7. Measured isentropic Mach number at midspan.

The local mainstream recovery temperature T_r is calculated from the local Mach number, upstream total temperature and a recovery factor based on the Prandlt number raised to the third power.

The heat transfer coefficient, defined by Eq. (1), measured by all gauges, each averaged over the steady portion of the run, is plotted against fraction of surface distance in Fig. 8 for the NGVs with both the cylindrical and fan-shaped hole geometries. Here the heat transfer coefficients for a solid blade (i.e. no film cooling) are plotted for comparison. The vertical lines in this figure (and the figures following) are the positions of the rows of film cooling holes. The data are averaged from three experiments. All experiments have been conducted at an

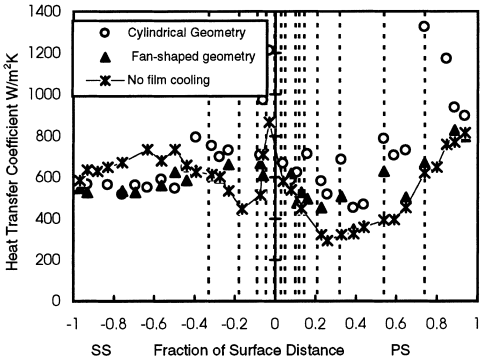

Fig. 8. Heat transfer coefficient for the cylindrical and fan-shaped cooling geometries. The solid NGV (no film cooling) is also shown. The vertical lines indicate the location of the film-cooling rows.

engine design condition, summarised in Table 1 and described in Section 3.1, and at a coolant-to-mainstream density ratio of 1.77.

The cylindrical-hole data will be discussed first. On the pressure surface the ejection of coolant into the turbulent boundary layer generally increases the heat transfer coefficient, with some significant local increases in regions immediately downstream of cooling rows as would be expected. The heat transfer rise caused by the laminar to turbulent transition is seen on the non film-cooled early suction surface data. This transitional region is not present when the film cooling is in operation as the coolant ejection trips the boundary layer. The heat transfer coefficient is largest in the shower-head region near the leading edge and falls progressively towards the back of the suction surface. Again the heat transfer coefficient near the film rows is higher than the uncooled case, but at about 50% surface distance the level drops below that of the uncooled case. This may be associated with a thicker boundary layer from the film cooling downstream of the last row on the suction surface.

Fig. 8 also compares the heat transfer coefficient for the fan-shaped and cylindrical geometries at the same coolant-to-mainstream pressure ratio. On the pressure surface the slower efflux of coolant through the fan-shaped holes has resulted in a lower heat transfer coefficient where compared with the cylindrical geometry. A similar pattern is exhibited on the suction surface. Downstream of the last film cooling row both film cooling geometries yield similar heat transfer coefficients.

Fig. 9 is a plot of cooling effectiveness as a function of surface distance for both the cylindrical and fan-shaped film cooling geometries. The effectiveness is seen to reach local peaks immediately downstream of each film cooling row. The data have been connected with a line to illustrate the general trend. A more dense concentration of gauges would provide more detailed information. This figure illustrates that despite the large number of film cooling holes near the leading edge, the effectiveness in this region is quite low. This may be associated with the high blowing rates in the shower head or stagnation region. On the pressure surface the effectiveness increases until about 80% surface distance. The effectiveness reaches a peak on the suction surface near 20% surface distance and decreases smoothly towards the trailing edge.

Fanning the holes results in a significant improvement of the cooling effectiveness in the region immediately downstream of the cooling holes. On the pressure surface, the fan-shaped geometry levels drop steeply further downstream, but the overall effectiveness is greater than that of the cylindrical geometry. On the suction surface the effectiveness measured using the fan-shaped hole geometry is consistently higher than that for the cylindrical geometry.

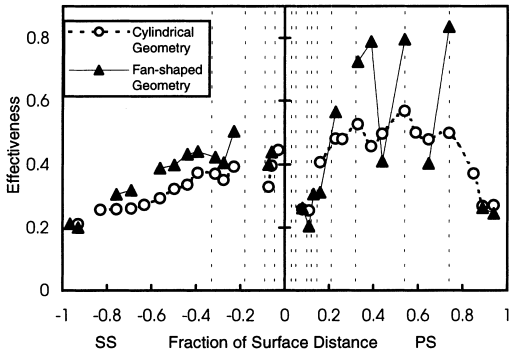

Fig. 9. Cooling effectiveness for cylindrical and fan-shaped film cooling geometries. The vertical lines indicate the location of the film-cooling rows.

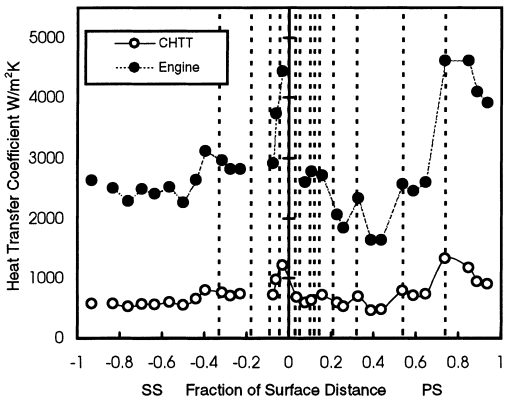

Fig. 10. Heat transfer coefficient corrected to engine conditions for cylindrical film cooling geometries. The vertical lines indicate the location of the film-cooling rows.

Figs. 10 and 11 compare the heat transfer coefficient and effectiveness for the cylindrical film cooling holes which would exist at engine conditions with those measured in the CHTT using the transformation in Eqs. (4) and (7). For these figures the local conductivity and specific heats of the foreign gas and mainstream air at 300 K have been modified to those which would exist with air coolant at 1000 K and mainstream flow at 1800 K. The change in axial chord dimension (the CHTT is at 1.4 times engine scale) has also been taken into account.

These figures demonstrate that care must be taken when undertaking experiments using foreign gases which have thermal properties which differ from those being modelled. The experiments have correctly modelled the film cooling aerodynamics and the spatial distribution of coolant. Thus they are of benefit not just for CFD code validation but also directly to the engine designer.

6. Conclusions

Thin-film technology has been used to measure the heat transfer coefficient and cooling effectiveness over heavily film cooled nozzle guide vanes. The measurements were performed in a transonic annular cascade at engine-representative Mach and Reynolds numbers. The paper identifies the important parameters for simulating film cooling and points out that the

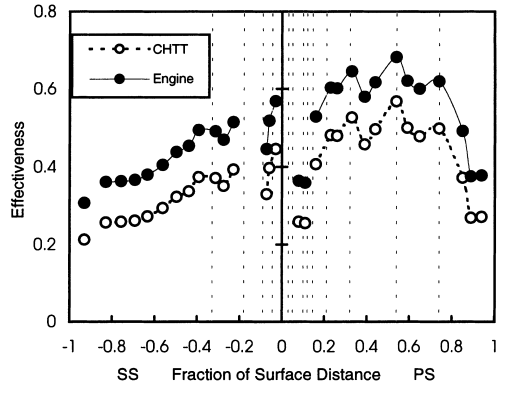

Fig. 11. Cooling effectiveness corrected to engine conditions for cylindrical film cooling geometries. The vertical lines indicate the location of the film-cooling rows.

coolant-to-mainstream density ratio can be simulated using a foreign gas mixture which has the same ratio of specific heats as air. The simulation of the correct flow field provides valuable validation data for CFD codes. Furthermore, it has been demonstrated that engine-levels of heat transfer coefficient and effectiveness can be deduced if thermal properties of the mainstream and coolant gases are taken into account.

Acknowledgements

This work was funded by Rolls Royce plc, the Defence Evaluation and Research Agency (DERA), MoD and DTI. The authors are grateful for the assistance of D.A. Rowbury, C.R.B. Day and T. Godfrey.

References

Butler, R.J., Baugh, J.W., 1996. The effect of the thermal boundary condition on transient method heat transfer measurements on a flat plate with a laminar boundary layer. Journal of Heat Transfer 118, 831–837.

Cho, H.H., Goldstein, R.J., 1995. Heat (mass) transfer and film cooling effectiveness with injection through discrete holes: Part II – On the exposed surface. ASME Journal of Turbomachinery 117, 451–460.

Doorly, J.E., Oldfield, M.L.G., 1987. The theory of advanced multilayer thin film heat transfer gauges. International Journal of Heat Mass Transfer 30 (6), 1159–1168.

Drost, U., Bolcs, A., Hoffs, A., 1997. Utilization of the transient liquid crystal for film cooling effectiveness and heat transfer investigations on a flat plate and a turbine airfoil. ASME Paper 97-GT-26.

Eckert, E.R.G., Hartnett, J.P., Birkebak, R., 1957. Simplified equations for calculating local and total heat flux to nonisothermal surfaces. Journal of Aeronautical Sciences 24 (7), 549–550.

Friedrichs, S., Hodson, H.P., Dawes, W.N., 1995. Distribution of film-cooling effectiveness on a turbine endwall measured using the ammonia and diazo technique. ASME Paper 95-GT-1.

Giebert, D., Gritsch, M., Schultz, A., Wittig, S., 1997. Film cooling from holes with expanded exits: A comparison of computational results with experiments. ASME Paper 97-GT-163.

Goldstein, R.J., 1971. Film cooling. Advances in Heat Transfer 7, 321–379.

Goldstein, R.J., Eckert, E.R.G., Ramsey, J.W., 1968. Film cooling with injection through holes: Adiabatic wall temperatures downstream of a circular hole. ASME Journal of Engineering for Power 384–395.

Guo, S.M., Spencer, M.C., Lock, G.D., Jones, T.V., Harvey, N.W., 1995. The application of thin film gauges on flexible plastic substrates to the gas turbine situation. ASME Paper 95-GT-357.

Hartnett, J.P., 1985. Mass Transfer Cooling. In: Handbook of Heat Transfer Applications, Chapter 1. McGraw Hill, New York.

Haslinger, W., Hennecke, D.K., 1996. The ammonia and diazo technique with CO_2 calibration for highly resolving and accurate measurement of adiabatic film cooling effectiveness with application to a row of holes. ASME Paper 96-GT-438.

Hay, N., Lampard, D., 1995. The discharge coefficient of flared film cooling holes. ASME Paper 95-GT-15.

Hay, N., Lampard, D., Saluja, C.L., 1984. Effects of cooling films on the heat transfer coefficient on a flat plate with zero mainstream pressure gradient. ASME paper 84-GT-40.

Jones, T.V., 1991. Definition of heat transfer coefficient in the turbine situation. Symposium on Turbomachinery: Latest Developments in a Changing Scene. IMechE Paper C423/046.

Jones, T.V., 1995. The thin film heat transfer gauge – A history and new developments. Invited Lecture, Fourth National UK Heat Transfer Conference, Manchester. IMechE Conference Transactions C510/150/95, pp. 1–12.

Jones, T.V., 1998. Theory for the use of foreign gas in simulating film cooling. Symposium of the NATO Applied Vehicle Technology Panel on Design Principles and Methods for Aircraft Gas Turbine Engines.

Jones, T.V., Oldfield, M.L.G., Ainsworth, R.W., Arts, T., 1993. Transient-cascade testing. In: Advanced Methods for Cascade Testing, Chapter 5. AGARD AG-328.

Martinez-Botas, R.F., Lock, G.D., Jones, T.V., 1995. Heat transfer measurements in an annular cascade of transonic gas turbine blades using the transient liquid crystal technique. ASME Journal of Turbomachinery 117 (3), 425–431.

Meece, C.E., 1995. Gas turbine technologies of the future. ISABE 95-7006.

Oldfield, M.L.G., Jones, T.V., Schultz, D.L., 1978. On-line computer for transient turbine cascade instrumentation. IEEE Transactions on Aerospace and Electronic Systems AES, 5.

Oldfield, M.L.G., Burd, H.J., Doe, N.G., 1984. Design of wide-bandwidth analogue circuits for heat transfer instrumentation in transient tunnels. In: Metzger, D.E., Afga, N.H. (Eds.), Heat and Mass Transfer in Rotating Machinery. 16th Symposium of the International Centre for Heat and Mass Transfer, Dubrovnik, 1982. Hemisphere, Washington, DC.

Oldfield, M.L.G., Guo, S.M., 1997. Aero-thermal properties of foreign gas (SF6/Ar) and air: Recommended formulae from 160-1000K. OUEL Report 2141/97.

Richter, J., Jung, K., Hennecke, 1996. An investigation of heat transfer by leading edge film cooling applying the naphalene sublimation technique. ASME Paper 96-GT-463.

Schultz, D.L., Jones, T.V., 1973. Heat transfer measurements in short-duration hypersonic facilities. AGARD AG-165.

Spencer, M.C., Jones, T.V., Lock, G.D., 1996. Endwall heat transfer measurements in an annular cascade of nozzle guide vanes at engine representative Reynolds and Mach numbers. International Journal of Heat and Fluid Flow 17, 139–147.

Teekaram, H.J.A., Forth, C.J.P., Jones, T.V., 1989. The use of foreign gas to simulate the effects of density in film cooling. Transactions of the ASME Journal of Turbomachinery 111, 57–62.